Title	Stabilization of self-focusing instability in wide-aperture semiconductor lasers
Authors	Voignier, Vincent;Houlihan, John;O'Callaghan, J. R.;Sailliot, C;Huyet, Guillaume
Publication date	2002
Original Citation	Voignier, V., Houlihan, J., O'Callaghan, J. R., Sailliot, C. and Huyet, G. (2002) 'Stabilization of self-focusing instability in wide-aperture semiconductor lasers', Physical Review A, 65(5), 053807 (5pp). doi: 10.1103/PhysRevA.65.053807
Type of publication	Article (peer-reviewed)
Link to publisher's version	https://journals.aps.org/pra/abstract/10.1103/PhysRevA.65.053807 - 10.1103/PhysRevA.65.053807
Rights	© 2002, American Physical Society
Download date	2025-08-17 19:20:42
Item downloaded from	https://hdl.handle.net/10468/4560

Stabilization of self-focusing instability in wide-aperture semiconductor lasers

V. Voignier, J. Houlihan, J. R. O'Callaghan, C. Sailliot, and G. Huyet

Physics Department, National University of Ireland, Cork, Ireland

A mechanism for the stabilization of the output of filamentary broad-area edge-emitting semiconductor lasers is analyzed experimentally and theoretically. This mechanism occurs when the carrier density is profiled in the transverse direction. The laser structure consisted of a wide-aperture edge-emitting laser diode operating in pulsed mode to avoid thermal guiding effects. The injection current profile was modified from the usual step-function case to a Lorentzian-like profile through the inclusion of a 10 μm p-type epitaxial spreading layer. The resulting nonlinear transverse mode is described and the possibility of its observation in two transverse dimensions is discussed.

I. INTRODUCTION

The analysis of transverse structures of optical systems has been the subject of many studies to investigate pattern formation when spatial diffusion remains small compared to diffraction [1]. Experimental studies include sodium vapors [2], liquid-crystal valves [3], photorefractive crystals [4,5], optical parametric oscillators [6], and large-aspect-ratio lasers such as carbon dioxide [7–9] or semiconductor lasers [10,11]. In semiconductor lasers, the curvature of the valence and conduction bands lead to a carrier-dependent refractive index [12]. In general, the refractive index decreases as the carrier density increases. As a result, any localized depletion of the carrier density creates a waveguide which focuses the light and causes further depletion of the (local) carrier density. This self-focusing mechanism generates high-brightness, unstable filaments of light [13–15] which are similar to the Benjamin-Feir instability observed within the Ginzburg-Landau equations [16]. In semiconductor lasers, this unstable self-focusing deteriorates the spatial coherence of the beam. Moreover, the presence of high-intensity filaments of light can also lead to catastrophic optical damage at the laser facet [17]. There have been three main approaches taken to suppress these instabilities. The first involves modifying the material structure to reduce the phase-amplitude coupling with, for example, quantum dot materials [18] or by introducing strain [19]. A second approach relies on the modification of the laser resonator [20–23]. Yet another approach uses a spatially varying pump profile to reduce the onset of filamentation [24]. In this paper, we first present a method to achieve such a spatially varying pump profile, before describing the experimental results and the underlying theory.

II. EXPERIMENTAL REALIZATION OF SPATIALLY VARYING PUMP PROFILE

Current profiling is an attractive control technique as it does not require complex material growth or laser processing techniques. It has been implemented through the use of a patterned electrode [24] or inclusion of an extra spreading layer [25,26]. Experimental current profiling was achieved here using the latter technique as shown in Fig. 1. The re-

sulting current profile shape can be determined from the spontaneous emission profile below threshold. As can be seen in Fig. 2 the current profile is modified from the usual top-hat injection to a smooth bell-shaped profile [full width at half maximum (FWHM) 80 μm from a 5 μm contact stripe]. However, as well as increasing carrier spreading, this modification of the material structure resulted in increased Ohmic heating because of an increase in the series resistance of the laser. This heating profile can result in a thermally induced refractive index profile which may induce instabilities in the optical field. To avoid these heating effects in the study of current profiling we excited the laser with electrical pulses. The width of the electrical pulse was 100 ns, which is long enough to capture the full carrier-field interaction while avoiding thermal issues. The resulting near- and far-field distributions are shown in Fig. 2. Generally, the near field was single lobed while the far field consisted of two lobes symmetrically placed about the optic axis. This behavior persisted from the onset of lasing up to ten times threshold.

To examine the relationship between near- and far-field intensity profiles, we reimaged the near field associated with different parts of the far field [27]. Thus, a spatial filter was inserted in the far field before reimaging the near field onto a photodiode array. The lens used had a focal length several times the Raleigh length of the device (numerical aperture 0.28, $f = 14.5$ mm); thus the plane of the lens was approximated to the far field and spatial filtering could be performed just after the lens. As the spatial filter was introduced, we observed that each lobe of the far field was associated with one-half of the near field, as shown in Fig. 3. Generally, we
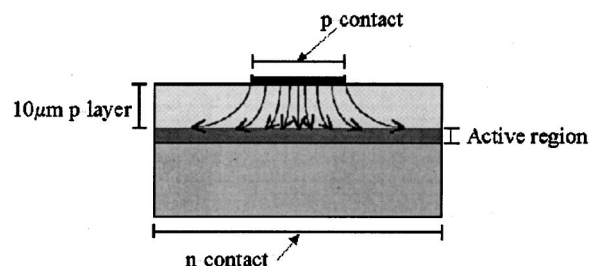

FIG. 1. Cross section of the p spreading layer device. The thick p layer allows the carriers to spread, thus smoothing the injection profile in the active region.
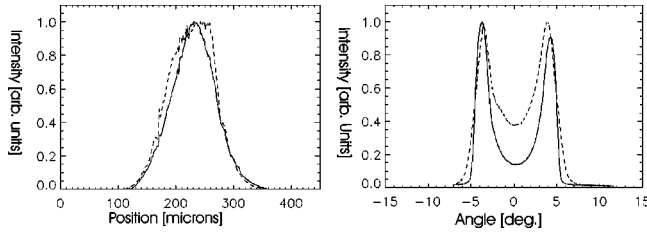
FIG. 2. Laser characteristic near fields [left, below threshold (dashed) and above threshold (solid)] and far fields [right, just above threshold (dashed) and ten times threshold (solid)]. In the pulsed regime (100 ns pulses), the single-lobed near field results in a double-lobed far field.

also observe some modulation in the reimaged near-field intensity, whose frequency can be varied with filter position. As each lobe in the far field is off axis, the near field can be decoupled into two spatially distinct counterpropagating traveling waves. Furthermore, we have no crossing over of the spatially distinct optical fields as they propagate from near to far field, i.e., light from the left side of the laser forms the left lobe of the far field, and vice versa. Thus, these traveling waves are generated in the center of the pumped region and propagate toward the edges.

The near field was then resolved into its longitudinal mode components to determine how different longitudinal modes couple to generate these spatial patterns. As shown in [27], each longitudinal mode displays the same spatial behavior as the total near field and thus we conclude that this transverse traveling-wave selection is independent of the multilongitudinal mode nature of the laser. We note that the beam can be focused down to to a well-defined spot which corresponds to a virtual source point of 5 μm (Fig. 4). To investigate the level of coherence between the two traveling waves in the near field (and hence the two lobes in the far field), we used a Michelson interferometer to interfere one lobe with the other. The results are shown in Fig. 4. The high visibility of the interference fringes indicates a high level of coherence between the two traveling waves.

III. THEORETICAL MODEL

Several schemes to model broad-area semiconductor lasers have been presented in the literature, each differing in
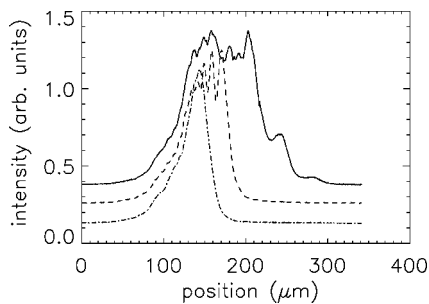

FIG. 3. Reimaged near fields when a spatial filter is progressively inserted in the far field from the right side. Top: total near field. Middle: all of the right lobe is cut. Bottom: all of the right lobe and part of the left lobe are cut. This demonstrates the spatial interdependence between the near and far fields.
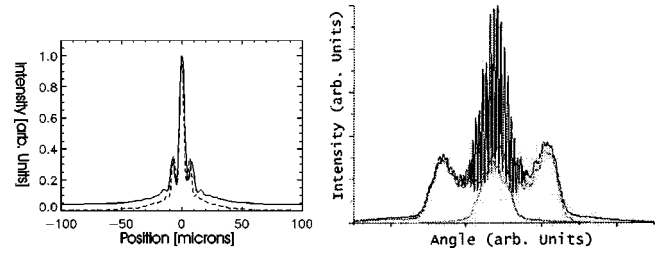

FIG. 4. Focusing properties of the current spreading laser (left) and demonstration of coherence between two far-field lobes using a Michelson interferometer (right).

the level of approximation. A full description of the system involves using many-body theory at a microscopic level to model material response and a fully space-time-resolved wave equation [28]. A commonly used approximation is to describe the material frequency response and the phase-amplitude coupling nonlinearity at a macroscopic level [29]. Furthermore, if longitudinal mode dynamics are unimportant (which, as mentioned earlier, is the case here), the wave equation can be integrated in time and transverse spatial coordinates alone [30]. Our approach will follow the latter scheme. A Lorentzian gain curve was used since experimentally lasing occurs only in a few modes located at the peak of the gain. This model is based on Maxwell-Bloch equations, where a term has been added to take into account nonlinearities associated with the linewidth enhancement factor, and where the pump current depends on the transverse coordinates. Furthermore, the model neglects carrier transport within the active region [31].

In a dimensionless form, the equations read

$$\partial_t E = -\kappa \left[1 - i\delta + i\alpha(D-1) - i\frac{a}{2}\nabla_{\mathbf{r}}^2 \right] E - \kappa P,$$

$$\partial_t P = -\gamma_\perp [DE + (1+i\delta)P], \tag{1}$$

$$\partial_t D = -\gamma_\parallel [-\tfrac{1}{2}(E^*P + EP^*) + D - j(\mathbf{r})],$$

where $\mathbf{r}$ is the transverse coordinate vector, $E(\mathbf{r})$ is the complex amplitude of the longitudinal mode, $P(\mathbf{r})$ is the complex polarization of the medium, $D(\mathbf{r})$ is the population inversion, $j(\mathbf{r})$ is the normalized pump profile, κ, $\gamma_\perp$, and $\gamma_\parallel$ are, respectively, the field, polarization, and inversion decay rates, δ is the cavity detuning, α accounts for the phase-amplitude coupling, $\nabla_{\mathbf{r}}^2$ is the transverse Laplacian, and a is the diffraction parameter. We set $\delta = 0$ (perfect cavity resonance). Unless otherwise stated, the results presented here used the following parameters: $\kappa = 1$ (the time unit in the model is 1 ps), $\alpha = 4$, $a = 1$ (the length unit in the model is 5 μm), $\gamma_\perp = 10$, and $\gamma_\parallel = 5 \times 10^{-3}$. These parameters are typical for semiconductor lasers.

To understand the spatiotemporal complexity of semiconductor lasers, we note that these equations can be reduced to

$$\partial_t E = -\kappa \left[1 - \frac{J(\mathbf{r})}{1 + |E|^2} + i\alpha \left(\frac{J(\mathbf{r})}{1 + |E|^2} - 1 \right) - i\frac{a}{2}\nabla_{\mathbf{r}}^2 \right] E,$$
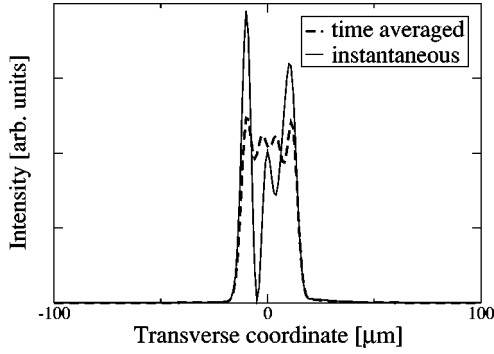
FIG. 5. Simulated instantaneous (solid) and time-averaged (dashed) optical fields of step-function laser displaying filamentary dynamics.

when the polarization and carrier dynamics are eliminated either adiabatically or by multiscale analysis. In the latter case, which is commonly carried out just above threshold, we have $1/(1+|E|^2) \simeq 1 - |E|^2$, which reduces the above equation to the complex Ginzburg-Landau equation. This generic equation describes many nonlinear systems and most dynamical laser models can be reduced to it with adequate approximations. For a constant-current profile, this equation does not have stable steady-state solutions due to the Benjamin-Feir instability [32].

IV. THEORETICAL RESULTS AND DISCUSSION

A. Broad-area laser

To describe broad-area edge-emitting lasers, Eqs. (1) were integrated over one transverse dimension with a square pump profile. When the laser operated above threshold filamentary dynamics ensued. Typical filamentation dynamics are depicted in Fig. 5 where the pump profile width was 40 μm. Although the intensity average does not vary greatly across the pumped region, the instantaneous intensity snapshot displays sharp peaks corresponding to unstable filaments. It is this filamentary dynamics which destroys the spatial coherence of the beam. These filaments are typically 5 μm wide and have a lifetime of the order of the relaxation oscillation time. This behavior has been experimentally observed in [14] and investigated theoretically in [15].

B. Profiled injection

The current profile used to model our laser was determined by the shape of the spontaneous emission profile below threshold (Fig. 2) and was approximated by a Lorentzian profile. The resulting near field consists of two spatially distinct counterpropagating transverse traveling waves generated at the center of the profile. These stable waves result in a single-lobed near-field intensity and double-lobe far-field intensity, each lobe being associated with one traveling wave (Fig. 6) as described in [27]. The wave vector of the traveling wave and thus the divergence of the far field were dependent on the α factor. Further agreement between simulation and experiment was obtained by reproducing theoretically the effect of spatial filtering in the far field on the near field. The results can be seen in Fig. 7.
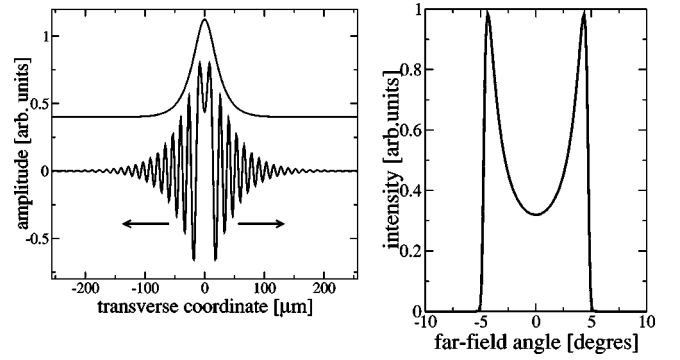

FIG. 6. Characteristic far field (right) and near field (left) resulting from a Lorentzian pumping profile in the simulation. The far-field intensity exhibits two lobes as in the experiment. The near field is composed of two counterpropagating traveling waves (bottom, real part of electric field) while its intensity (top) follows the pump profile.

The traveling-wave solution can be obtained by solving Eqs. (1) or the Ginzburg-Landau equation for monochromatic solutions [$E(x,t) = E(x)e^{i\omega t}$]. There is usually no analytical solution except in the special case of constant pump profile with the field fixed to zero at a point [33]. In our case, there is no analytical solution to our knowledge. However, if we assume the intensity profile of the laser follows the current profile we can qualitatively obtain traveling-wave solutions. As a result, the laser has a single-lobed near field with the associated double-lobed far field [34]. This demonstrates the existence of traveling-wave solutions but does not address their stability. The numerical integration of the Maxwell-Bloch equations demonstrates the stability of the traveling-wave solutions under profiled injection.

To further characterize the optical field, we numerically propagated the theoretical near field through a lens by integrating the Fresnel equations. This was also performed experimentally by placing a lens in the far field of the laser and a linear photodiode array at a fixed distance from the laser. The lens position in the propagation direction was controlled by a piezoelectric positioner. Individual scans of the transverse beam profile as the optical field propagated from the
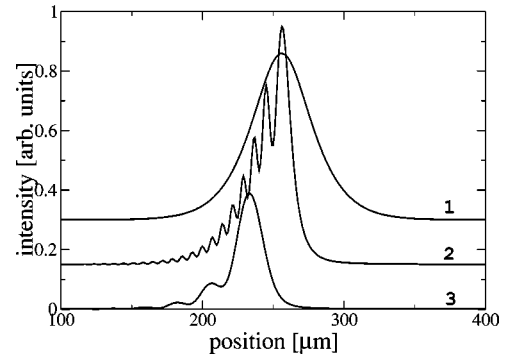

FIG. 7. Reformed near field after part of the far field of Fig. 6 has been removed (1, no filter; 2, angles greater than 3.4° removed; 3, angles greater than −2.3° removed). Note the appearance of fringes, whose frequency depends on the position of the filter, as seen in the experiment (Fig. 3).
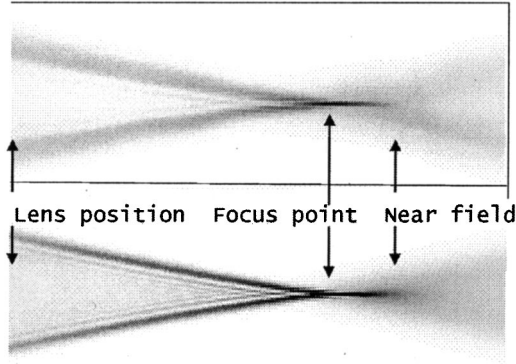
FIG. 8. Theoretical (bottom) and experimental (top) propagation of nonlinear mode from the far field at a lens (far left) through the focus point.

far field (at the lens) through the reimaged near field and onto the reimaged far field were acquired by varying the lens position and are compared with the theoretical case in Fig. 8. It has been shown experimentally and theoretically that this type of propagation can be used to fully reconstruct the optical phase and intensity profiles at the source [35] and thus contains all of the information about our beam (Fig. 9).

The mechanism for filamentation stabilization is the following: profiling the pump current induces a carrier density profile, which in turn induces an index profile through the phase-amplitude coupling term. Since the refractive index decreases with increasing carrier density, the index profile is antiguiding. This antiguiding profile prevents the formation of filaments by spreading intensity irregularities, the seeds of filamentation. Thus it counteracts the destabilizing self-focusing which occurs in the case of top-hat injection. To illustrate this mechanism, a background antiguiding index profile was introduced into the above model with a square injection profile. This index profile was implemented by considering the cavity detuning (δ) as a spatially varying parameter, i.e., $\delta = \delta_0 + \delta(x)$. This antiguiding profile was found to stabilize the usually unstable square injection profile.

C. Stability of profiled injection

We investigated the influence of different parameters on the stability of the traveling-wave solution. Increasing the
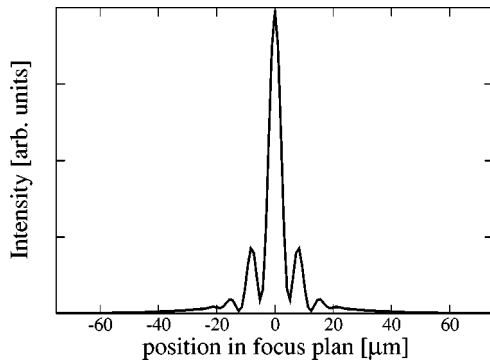

FIG. 9. Simulated focus point of nonlinear mode. Note the good overall agreement with experiment (Fig. 4).
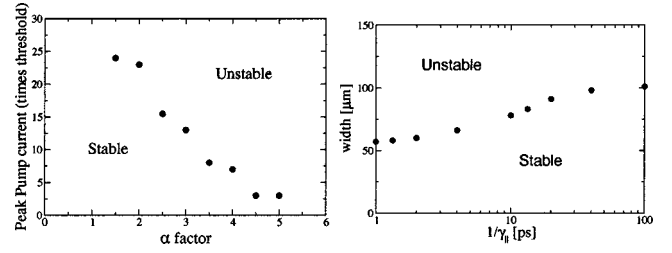

FIG. 10. Graphs depicting range of stability of nonlinear mode with respect to pump current and α factor (left) and profile width and inversion decay time (right).

peak pump of the profile, the width of the profile, or the self-focusing factor beyond a critical value will bring the laser into a filamentation regime (Fig. 10).

It is interesting to note that the profile shape determines the stability range. We looked at the critical profile width for different profile shapes (Lorentzian, Gaussian, triangular). For a maximum pump value of three times threshold and all other parameters as in Sec. III, the triangular was the most stable profile with a critical width (FWHM) of 160 μm followed by the Lorentzian (critical width 115 μm), and the least stable was the Gaussian (critical width 60 μm).

V. EXTENSION OF STABILIZATION MECHANISM TO TWO DIMENSIONS

Both experimental and numerical results previously presented are related to edge-emitting devices, i.e., one transverse dimension. It is interesting to consider how these results can be extended to the two-transverse-dimension case, e.g., vertical-cavity surface-emitting lasers (VCSELs). To describe VCSEL dynamics we integrated the model previously outlined (see Sec. III) over two spatial dimensions (2D). We compared a square profile with a cylindrically symmetric Lorentzian profile. In the case of the former the laser displayed complex filamentary dynamics similar to the one-dimensional case. In the case of the profiled injection, cylindrically symmetric traveling waves are observed in the laser near field, similar to those observed in the one-dimensional case. Those two cases are displayed in Fig. 11. However, since the stabilizing mechanism is based on antiguiding ef-
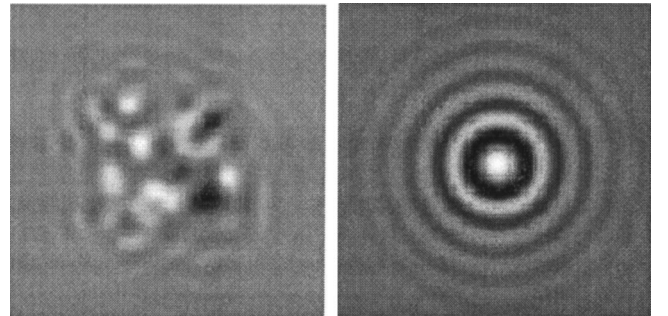

FIG. 11. Real part of the electric field of a 2D laser with a square (left) and Lorentzian (right) current profile, thus demonstrating nonlinear mode stabilization in two dimensions by current profiling.

fects, we should expect an increase in the diffraction losses of the gain-profiled laser in both one- and two-dimensional cases. This should result in an increase of the threshold current. To quantify the magnitude of this effect, we varied the antiguide strength by varying the α factor and measured the resulting increase in the threshold current. This increase in threshold is rather small in the one-dimensional case (50% for $0 < \alpha < 4$) but much larger for two transverse dimensions (100% for $0 < \alpha < 2$, both for a Lorentzian profile). No noticeable change in threshold current was observed when a square profile was used, in either one or two dimensions.

VI. CONCLUSION

In conclusion, we presented a mechanism for obtaining stable traveling waves in the transverse section of a semiconductor laser. This was illustrated with experimental and numerical results utilizing the technique of transverse current profiling. The stabilized laser field can be described as a single nonlinear transverse mode whose stability is limited by various factors, namely, temperature gradients, profile type and width, pump level, carrier lifetime, and phase-amplitude coupling. This mode was also demonstrated to be a stable solution in the two-transverse-dimension case (e.g., a VCSEL). The underlying physics of current profiling could be extended to the case of transversely coupled lasers to engineer phase-locked laser arrays.

[1] F. T. Arecchi, S. Bocaletti, and P. Ramazza, Phys. Rep. **318**, 1 (1999).

[2] T. Ackemann, Yu. A. Logvin, A. Heuer, and W. Lange, Phys. Rev. Lett. **75**, 3450 (1995).

[3] E. Pampaloni, P. L. Ramazza, S. Residori, and F. T. Arecchi, Phys. Rev. Lett. **74**, 258 (1995).

[4] F. T. Arecchi, G. Giacomelli, P. L. Ramazza, and S. Residori, Phys. Rev. Lett. **67**, 3749 (1991).

[5] K. Staliunas, G. Slekys, and C. O. Weiss, Phys. Rev. Lett. **79**, 2658 (1997).

[6] P. Lodahl, M. Bache, and M. Saffman, Phys. Rev. Lett. **85**, 4506 (2000).

[7] D. Dangoisse, D. Hennequin, C. Lepers, E. Louvergnaux, and P. Glorieux, Phys. Rev. A **46**, 5955 (1992).

[8] G. Huyet, C. Martinoni, J. R. Tredicce, and S. Rica, Phys. Rev. Lett. **75**, 4027 (1995).

[9] F. Encinas-Sanz, I. Leyva, and J. M. Guerra, Phys. Rev. Lett. **84**, 883 (2000).

[10] R. Lang, A. Larsson, and J. Cody, IEEE J. Quantum Electron. **27**, 312 (1991).

[11] S. P. Hegarty, G. Huyet, J. G. McInerney, and K. D. Choquette, Phys. Rev. Lett. **82**, 1434 (1999).

[12] W. W. Chow, S. W. Koch, and M. Sargent, *Semiconductor-Laser Physics* (Springer-Verlag, Berlin, 1994).

[13] P. Kirkby, A. Goodwin, G. Thompson, and P. Selway, IEEE J. Quantum Electron. **13**, 705 (1977).

[14] T. Burkhard, M. O. Ziegler, I. Fisher, and W. Elsasser, Chaos, Solitons Fractals **10**, 845 (1999).

[15] J. Marciante and G. Agrawal, IEEE J. Quantum Electron. **33**, 1174 (1997).

[16] I. S. Aranson and L. Kramer, Rev. Mod. Phys. **74**, 99 (2002).

[17] A. Mosser, E. Latta, and D. Webb, Appl. Phys. Lett. **55**, 1152 (1989).

[18] T. C. Newell, D. J. Bossert, A. Stintz, B. Fuchs, K. J. Malloy, and L. F. Lester, IEEE Photonics Technol. Lett. **11**, 1527 (1999).

[19] M. P. Mullane and J. G. McInerney, IEEE Photonics Technol. Lett. **12**, 1147 (2000).

[20] A. P. Bogatov, P. G. Eliseev, M. A. Man'ko, G. T. Mikaelyan, and Y. M. Popov, Sov. J. Quantum Electron. **10**, 620 (1980).

[21] S. A. Biellak, C. G. Fanning, Y. Sun, S. S. Wong, and A. E. Siegman, IEEE J. Quantum Electron **33**, 219 (1997).

[22] J. N. Walpole, Opt. Quantum Electron. **28**, 623 (1996).

[23] D. C. Sun, S. R. Friberg, K. Watanabe, S. Machida, Y. Horikoshi, and Y. Yamamoto, Appl. Phys. Lett. **61**, 1502 (1992).

[24] C. Lindsey, P. Derry, and A. Yariv, Electron. Lett. **21**, 671 (1985).

[25] P. O'Brien, P. M. W. Skovgaard, J. G. McInerney, and J. S. Roberts, Electron. Lett. **34**, 1943 (1998).

[26] J. R. O'Callahan, J. Houlihan, V. Voignier, G. Huyet, J. G. McInerney, B. Corbett, and P. O'Brien, IEEE Photonics Technol. Lett. (to be published).

[27] J. Houlihan, J. R. O'Callahan, V. Voignier, G. Huyet, and J. G. McInerney, Opt. Lett. **26**, 1556 (2001).

[28] J. Moloney, R. Indik, J. Hader, and S. Koch, J. Opt. Soc. Am. B **16**, 2023 (1999).

[29] J. K. White, J. V. Moloney, A. Gavrielides, V. Kovanis, A. Hohl, and R. Kalmus, IEEE J. Quantum Electron. **34**, 1469 (1998).

[30] J. Martin-Regalado, S. Balle, and N. B. Abraham, IEE Proc.: Optoelectron. **143**, 17 (1996).

[31] D. Mehuys, R. J. Lang, M. Mittelstein, J. Salzman, and A. Yariv, IEEE J. Quantum Electron. **23**, 1909 (1987).

[32] M. C. Cross and P. C. Hohenberg, Rev. Mod. Phys. **65**, 851 (1993).

[33] P. S. Hagan, SIAM (Soc. Ind. Appl. Math.) J. Appl. Math. **42**, 762 (1982).

[34] K. Petermann, Opt. Quantum Electron. **13**, 323 (1981).

[35] M. G. Raymer, M. Beck, and D. F. McAlister, Phys. Rev. Lett. **72**, 1137 (1994).